

Fiber-integrated phase change metasurfaces with switchable group delay dispersion

Tiago Martins^{1, 2†}, Yihao Cui^{3†}, Behrad Gholipour^{2, 3, 4*}, Jun-Yu Ou², Orlando Frazão¹ and Kevin F. MacDonald²*

T. Martins, O. Frazão

¹ INESC TEC and Department of Physics and Astronomy, Faculty of Sciences, University of Porto, Rua do Campo Alegre, 687, 4150-179 Porto, Portugal

B. Gholipour, J. Ou, K. F. MacDonald

² Optoelectronics Research Centre and Centre for Photonic Metamaterials, University of Southampton, Southampton, SO17 1BJ, UK

Y. Cui, B. Gholipour

³ Department of Electrical and Computer Engineering, University of Alberta, Canada, T6G 1H9

B. Gholipour

⁴ Department of Chemistry, University of Southampton, Southampton, SO17 1BJ, UK

† Contributed equally to this work

Corresponding author: bgholipo@ualberta.ca

Keywords: Metamaterials, group delay dispersion, chalcogenides, Optical fiber, phase change, non-volatile, reconfigurable

Abstract:

We report on the demonstration of a fiber-integrated non-volatile reconfigurable metasurface providing high-contrast group delay dispersion switching functionality, which may be engineered to operate at wavelengths across the near-infrared (telecoms) band. Light-induced amorphous-crystalline phase switching in a chalcogenide (germanium antimony telluride) metasurface only a fraction of a wavelength thick, fabricated on the end-facet of a single mode optical fiber, enables intensity and phase modulation of the guided wave at metasurface designated bands. Such devices present a range of opportunities in fiberized remotely programmable phase/intensity multiplexing and dynamic dispersion compensation for emerging telecommunications and data storage/processing applications, including in photonic neural network and neuromorphic computing architectures.

1 Currently, the field of photonic metamaterials is evolving from being a nanotechnology-
2 enabled paradigm for engineering new electromagnetic properties to the device and system
3 levels (metadevices and metasystems). A key recent advance has been the emergence of
4 reconfigurable metamaterials offering optical properties on demand that enable dynamic, on-
5 the-fly, moulding of light. Thusfar, application potential of active nanophotonic/metamaterial
6 concepts is largely untapped, especially in waveguide and fiber-based optical systems, where
7 a new generation of components including rapidly reconfigurable spatial channel multiplexers,
8 dispersion compensation devices, routers and memory elements with small physical footprints
9 could be realized^[1]. Today's data networks are largely optically opaque, consisting of electronic
10 nodes connected by point-to-point fiber-optic links, reliant upon a series of volatile optical-
11 electronic conversions and volatile switches to move information across the network. This
12 creates substantial data latency issues, thermal footprint and inflated power consumption
13 requirements. To date, the potential for optical fibers to manipulate light themselves remains
14 largely unrealized and unexploited in networks. Therefore, the solution to overcoming these
15 looming challenges, lies in the exploitation of fiber-integrated devices capable of all-optical
16 non-volatile switching across telecom frequencies. This will remove electronic bottlenecks by
17 enabling fully fiberized all-optical telecommunication networks. At the same time, there is
18 rapidly growing interest in radically different photonic network architectures for neuromorphic
19 (brain-inspired) computing and implementation of machine learning, which take advantage of
20 the inherent parallelism of photonic technologies and again require ultra-compact, integrated
21 elements for dynamic phase/amplitude modulation and optical memory^[2]

22 In this pursuit, during the past decade, there has been increasing research interest in
23 developing adaptive/tunable multimaterial optical fibres^[3], by combining planar and fiber
24 devices incorporating a wide range of material platforms through a variety of manufacturing
25 techniques^[4]. Functional media can be integrated with solid-core fiber and planar waveguides

generically in one of two ways, based either on evanescent coupling to the guided mode^[5] - whereby a material or structure is positioned on or within the optical near field of the waveguide side wall; or in-line coupling – whereby a thin film, nanostructure or device intercepts the path of the guided mode, e.g. via a micro-collimator assembly (as in many commercial optical fiber optical isolators, circulators, beam splitters, etc.) or direct fabrication on the cleaved end facet of the waveguide core (as in a variety of recent applications to nonlinear optics and sensing^[6]). The integration of functional thin films and devices on fiber tips is a highly promising approach currently being explored; giving rise to a number of recent demonstrations that can address applications in nonlinear optics and sensing^[6]. Fiber-tip integration relies on intercepting the guided light beam by directly placing the light-modulating medium in its propagation path (i.e. covering the core on the tip of a cleaved fiber). Here we show that all-optical fiber-integrated non-volatile memory components with switchable dispersion, operating across telecom frequencies, can be realized through the integration of photonic metasurfaces made from reconfigurable phase change chalcogenide semiconductors with single mode commercial optical fibers.

Photonic metasurfaces are artificial electromagnetic media nanostructured on the subwavelength scale. They present a highly flexible technology paradigm for engineering electromagnetic space and (actively) controlling the propagation of light and its interaction with matter. An extensive range of enhanced optical properties, including dynamically tunable/switchable and nonlinear functionalities, have been demonstrated at near-infrared and visible frequencies, in metamaterials and metasurfaces comprised of nanostructured plasmonic metals and high-index dielectrics^[7]. Recently, the field of photonic metamaterials has evolved from being a nanotechnology-enabled paradigm for engineering new electromagnetic properties to the device and system levels^[8] where practical devices for real world applications capable of field-deployment, can be realized through the integration of nanophotonic

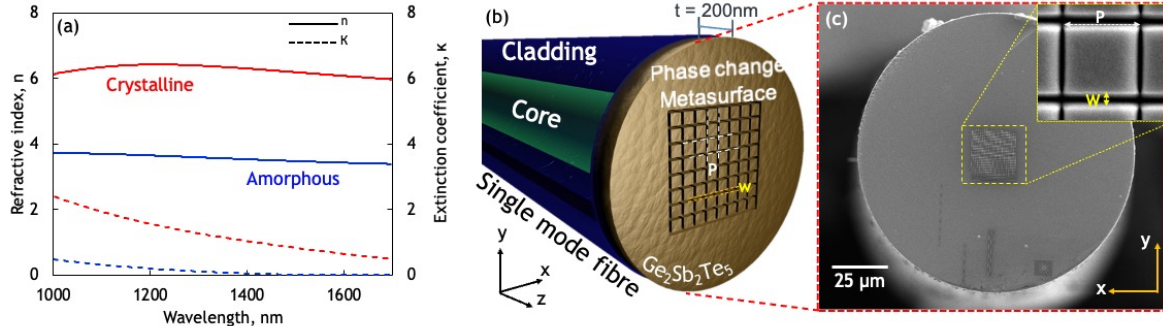


Figure 1. (a) Near-infrared spectral dispersion of the refractive index (n) and the attenuation coefficient (κ) of GST in the amorphous (blue) and crystalline (red) phases; (b) Schematic diagram of the fiber-integrated phase change metasurface optical switch based on a GST; (c) Scanning electron microscope image of the fiber metadvice; inset: detail of the cuboid GST metasurface structure.

metamaterials and metasurfaces with optical fiber technology. To this end, a large number of different material platforms are being explored for use in photonic metasurfaces, including noble plasmonic metals, conductive oxides, refractory nitrides, perovskite, chalcogenides and superconductors^[9]. Among them, chalcogenide semiconductors (alloys of sulphur, selenium and tellurium) present a uniquely flexible material platform that can be manufactured in various forms; optical fibers, thin films, nanoparticles and monolayers; and grown and patterned using CMOS compatible processes^[10]. They have been at the core of optical disk technology (DVDs/Blurays) and emerging memristive electronic random-access memory devices^[11]. However, they have much more to offer, aside from being good hosts for a variety of metallic and rare-earth dopants, they present a number of compositionally tunable properties^[12], from photo-conduction and infrared transparency to high optical nonlinearity and photorefractivity^[13]. Notably, the spectral dispersion of their response to electromagnetic fields is compositionally-controllable and spans a wide range of regimes (plasmonic, low and high refractive index)^[14]. Therefore, such materials can provide for a variety of unusual and intriguing electromagnetic wave and light-matter interaction phenomena across ultraviolet (UV) to infrared IR frequencies. They can also exhibit heat/current/light-induced non-volatile,

1 reversible switching between optoelectronically distinct amorphous and crystalline phase states,
2 leading to substantive broadband changes in refractive index on femtosecond to nanosecond
3 timescales^[15].

4 Germanium antimony telluride ($\text{Ge}_2\text{Sb}_2\text{Te}_5$ or GST), as employed in this work, is a high-
5 index dielectric in both its amorphous and crystalline states across the near-infrared spectral
6 range. The amorphous to crystalline transition here entails an increase in the real part of the
7 refractive index along with an associated increase in extinction coefficient (Fig. 1(a)). The high
8 refractive index and index contrast between phase states offered by GST at infrared
9 wavelengths has been harnessed in the realization of thermally switchable hyperbolic
10 metamaterials as well as laser-rewritable and electrically switchable ‘all-dielectric’, plasmonic
11 and hybrid metasurfaces^[16]. In the visible range, crystalline GST is plasmonic (metallic), and
12 phase switching can thus be engaged to turn the plasmonic resonances of all-chalcogenide
13 metasurfaces on/off^[17].

14 GST films with a thickness $t = 200$ nm are deposited on cleaved single mode optical fibers
15 with a core size of $8\text{ }\mu\text{m}$ (Thorlabs SM980-5.8-125), by RF sputtering. A base pressure of $2 \times$
16 10^{-4} mbar is achieved prior to deposition and high-purity argon is used as the sputtering gas (70
17 ccpm to strike, 37 ccpm to maintain plasma). The fibers are held within 10 K of room
18 temperature on a rotating platen 150 mm from the target to produce low-stress amorphous, as-
19 deposited films. Sub-wavelength period (i.e. non-diffractive) cuboids, with a fixed linewidth
20 $W=80$ nm and periods P ranging from 900 to 1000 nm, each covering an area of approximately
21 $15\text{ }\mu\text{m} \times 15\text{ }\mu\text{m}$ ($\sim 2\times$ larger than the core diameter), were etched through the GST layer by
22 focused ion beam (FIB) milling, as illustrated in Figs. 1(b) and (c). During processing, special
23 care is taken to align the nanostructured area over the fiber core, ensuring experimental light
24 measurements reflect the interaction of light with the structured medium fabricated on the tip
25 of the fiber. The transmission characteristics of the fiberized devices were subsequently

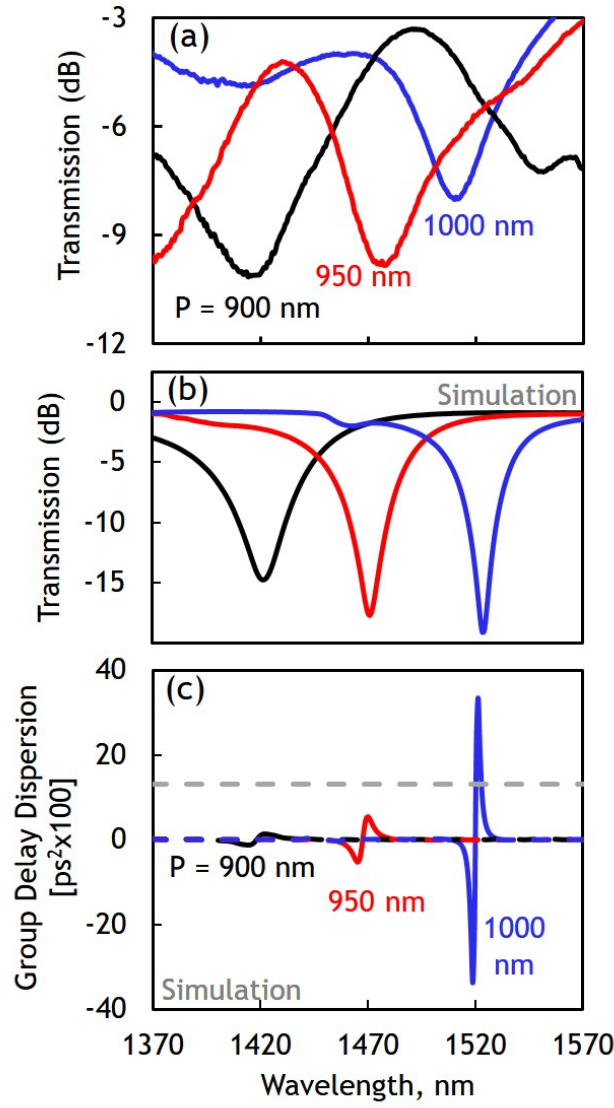


Figure 2. (a) Experimentally measured and (b) simulated transmission spectra for arrays of GST cubes with $w = 80$ nm, $t = 200$ nm and P taking three different values: 900, 950 and 1000 nm; (c) corresponding simulated spectral profile of the Group Delay Dispersion (GDD); the grey dashed line identifies the level of dispersion introduced by 1 m of single-mode telecom fiber (considering a fiber group velocity dispersion of 20 ps/nm.km); the black, red and blue dashed traces show the off-resonance GDD for arrays with $P = 900$, 950 and 1000 nm, respectively.

- 1 measured by focusing near-IR light ($1000 \leq \lambda \leq 1750$ nm) from a broadband light source
- 2 (Thorlabs SLS201L) onto the nanostructured fiber tip surface using a near-IR objective
- 3 (Mitutoyo M Plan Apo NIR 10x; NA = 0.26) and collecting the output using an Optical
- 4 Spectrum Analyzer (Ando AQ-6315E).

Fig. 2(a) shows the normalized (relative to an unstructured GST-coated fiber tip) measured transmission spectra of three fiber-integrated phase change metasurfaces with periods 900, 950 and 1000 nm. These show transmission resonances with spectral positions dependent upon the period of the nanostructured cuboids. Fig. 2(b) presents the simulated transmission spectra corresponding to three different periods of GST metasurfaces in their as-deposited amorphous phase with the same geometry as those experimentally fabricated. The simulations were run using a finite difference time domain solver (Lumerical FDTD Solutions). The model assumes a lossless non-dispersive silica substrate with refractive index of 1.45 (representing the single mode optical fiber) and uses ellipsometrically measured values of the complex permittivity for GST, as presented in Fig. 1(a). In addition, normal-incidence illumination using a plane-wave is considered. By virtue of periodic boundary conditions, an infinite array of GST cuboids in the x and y planes is simulated. There is good agreement between experimentally measured and numerically simulated transmission spectra. Therefore, owing to the fact that the nanostructured GST covers an area of the fiber tip surface far greater in size than the core, considering a simple geometry for our model consisting of a periodic array of GST cuboids on top of a silica substrate with refractive index equal to that of the fiber core is found to be sufficient in establishing a good qualitative and quantitative representation of the fiber-tip-integrated experimental device characteristics. Minor discrepancies are found to be related to manufacturing imperfections, i.e. deviations from the ideal model geometry such as slight over-milling of etched lines into the substrate, and the tapered/rounded cross-sectional profile of milled lines; and to possible contamination/stoichiometric drift in the GST layers during FIB milling, which may slightly modify refractive index.

The resonant response of the metasurface presents opportunity for spectral phase modulation at structurally engineered wavelength bands dictated by the metamolecule geometry. The group delay dispersion (GDD) is shown in Fig. 2(c). Group delay dispersion is

the second derivative of the change in spectral phase with respect to wavelength given by the equation:

$$GDD = \frac{\lambda^3}{2(\pi c)^2} \left[\frac{d\phi}{d\lambda} + \frac{\lambda}{2} \frac{d^2\phi}{d\lambda^2} \right]$$

where λ is the wavelength, c is the speed of light in vacuum, and ϕ is the spectral phase. Here, the phase and transmission for each metasurface in both amorphous and crystalline phases, across the spectral range of $\lambda = 1370\text{nm}$ to 1570nm , were extracted from Lumerical FDTD and imported into MATLAB for processing. Within the FDTD environment, the grating s parameter analysis group was utilized to obtain both transmission and phase data through the complex scattering parameter S_{21} . As longer periods are considered, and keeping in with the ensuing enhanced Q-factors linked to the transmission dips, higher maximum absolute GDD is attained for metasurfaces with $P = 1000\text{ nm}$, showing 0.33 ps^2 as the highest possible numerically simulated GDD. Positive (normal) and negative (anomalous) GDD values can also be engineered around the resonant spectral position. While outside the scope of the current study, GDD and phase delay in optical fiber integrated devices may also be measured experimentally using two-arm interferometric fiber network measurements.

The amorphous-to-crystalline transition in chalcogenides is an annealing process that can be instigated through heating the material to a temperature above the material's glass-transition point T_g ($\sim 160^\circ\text{C}$ for GST), but below its melting point T_m (600°C). The reverse transition, a melt-quenching process can be driven by shorter higher energy pulsed excitation that momentarily brings the material to a temperature above T_m . To evaluate the performance of our device in both structural phases, the fiber-integrated metasurfaces are illuminated with CW laser light at $\lambda=1550\text{ nm}$, which thermally anneals the surface area overlapping the fiber core, where the metasurface is fabricated. Reflectivity of the metasurface/fiber interface is monitored (through the fiber, via a circulator; an increase in reflectivity at 1550 nm being indicative of

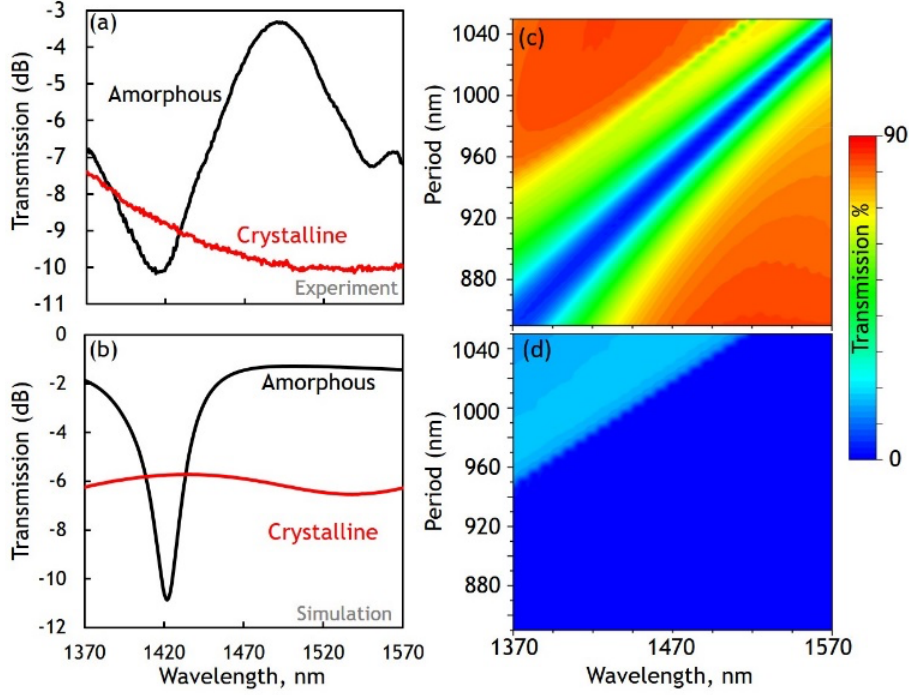


Figure 3. (a) Measured and (b) simulated transmission spectra for a metasurface with $w = 80$ nm, $t = 200$ nm and $P = 900$ nm, in the amorphous (black) and crystalline (red) phases; Along with corresponding numerically simulated transmission of metasurfaces ranging from 850nm to 1050nm periods in (c) amorphous and (d) crystalline states, with resonances covering the E, S and C telecommunication bands.

1 GST crystallization). This experimental configuration enables light-induced crystallisation of
 2 the GST metasurface via the fiber, i.e. in a manner compatible with remotely programmable
 3 fiber-integrated device architectures.

4 The changes in the spectral dispersion of transmission resulting from the crystallisation of
 5 the nanostructured GST metasurface are presented in Fig. 3, with corresponding numerical
 6 simulations of the expected transmission change presented in Fig. S1. The transition from the
 7 amorphous to the crystalline state involves an increase in the real part of the GST refractive
 8 index which results in a red-shift and substantial broadening of the resonant feature, rendering
 9 it almost imperceptible. This is accurately reproduced in corresponding numerical simulations
 10 (Figs. 3 (a), (b)). While the corresponding increase in the imaginary part of the GST refractive

index brings about a decrease in average transmission of the device across the spectral range under investigation and a broad flattening of the resonance feature. It should be noted that as stated previously phase transitions are instigated using a coupled CW laser light at $\lambda=1550$ nm, which thermally anneals the surface area overlapping the fiber core, where the metasurface is fabricated. In simulations this is assumed as a perfectly uniform spatially distributed phase transition, however in reality, this will create a randomly distributed mixture of slightly different clusters with different levels of crystallinity in the metasurface, which translates to the slight discrepancy seen in the crystalline phase simulations.

Numerically simulated field maps display the spatial profiles of the electric field in the metasurfaces (Figs. S2 (a) and (b)), alongside the magnetic field (Figs. S2 (c) and (d)), along a vertical plane cutting through the GST cuboids in both fully amorphous and crystalline phases of the GST layer. These field profiles help to characterize the resonances harboured by the proposed reconfigurable fiber-tip-integrated nanostructures. In a closed packed metasurface array arrangement, the observed resonance is seen to arise from the collect mode of the array. Therefore, the electric field can be seen mostly confined to the gap between cuboids (either in the silica substrate or constrained to the air/GST interface), with little electric field intensity confined inside the GST layer. The field maps in Figs. S2 (c, d) demonstrate that, for both the electric and magnetic fields, the variation in optical parameters associated with the structural phase transition induced in the GST film leads to a change in the spatial distribution of electric and magnetic field intensity confined in the GST layer as well as at the GST/air and silica interfaces.

As Fig. 4 (a) exemplifies, by changing the phase of the GST layer in a structure with $P = 900$ nm, the considerable phase modulation observed in the amorphous state is rendered almost imperceptible after crystallization. Consequently, the GDD collapses, being reduced from a maximum absolute value of 0.013 ps^2 in the amorphous state down to a maximum of 0.0021

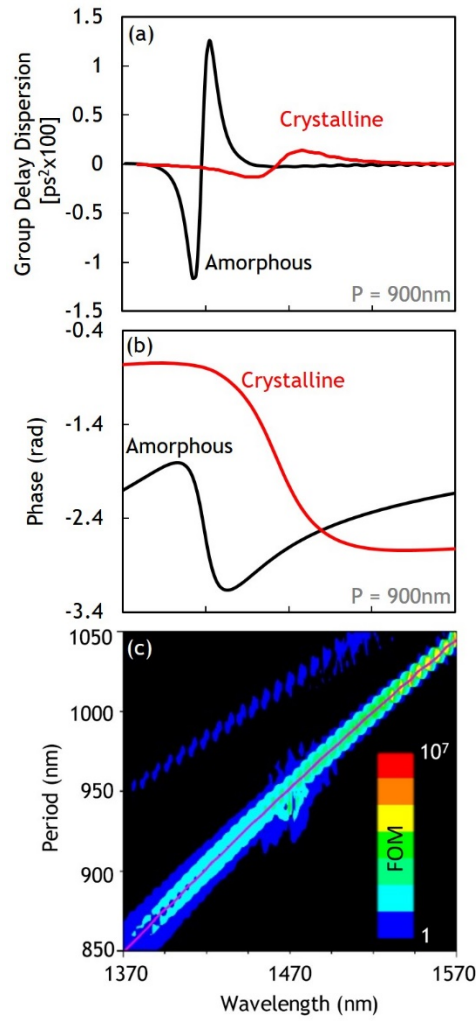


Figure 4. (a) Numerically simulated group delay dispersion (GDD) for amorphous and crystalline states of a metasurface with $w = 80$ nm, $t = 200$ nm and $P = 900$ nm, along with corresponding (b) phase. (c) Figure of Merit calculated for metasurfaces with periods ranging from 850nm to 1050nm. The colour black indicates $\text{FOM} = 0$. Magenta line indicates region where $T_A = T_C$.

- 1 ps^2 upon crystallization. This change in GDD translates to a substantial change in the optical
- 2 phase of a propagating signal as shown in Fig. 4 (b). With a view to practical applications a
- 3 figure of merit (FOM) is defined, relating the change in transmission (T) of a given signal with
- 4 the change in GDD upon structural phase transition (A and C denote amorphous and crystalline
- 5 phases respectively):

$$Performance\ Metric = \frac{|GDD_A - GDD_C|}{|T_A - T_C|}$$

In such a representation, the higher the performance metric, the higher the capability of the fiber integrated metasurface to introduce a large change in dispersion accompanied by a small change in the amplitude of the transmitted signal. As shown in Fig. 4(c), the highest performance metric is observed at the spectral position of the resonance wavelengths for a given metasurface. This can be tuned from the E to C telecom bands by changing the period of the cuboid metamolecule and shows a gradual increase at higher wavelengths due to the reduced losses in the GST layer which brings about an increase in the quality-factor of the resonant feature. It should be noted that at positions where $T_A = T_C$, the performance metric will yield high values that tend to infinity. These regions have been clearly indicated in Figure 5c.

In conclusion, we have demonstrated reconfigurable phase change metamaterials with intensity and dispersion switching capability nanofabricated directly on the tip of silica optical fibers. Such devices can be mechanically spliced to existing networks enabling the merging of the optical fiber and reconfigurable metamaterial fields into a single robust monolithic device platform free from alignment issues and ready for commercialization and integration in global telecommunication networks, drastically reducing physical footprint, data latency, bottlenecks and power consumption in such devices. Specifically, this work establishes a new device platform for non-volatile all-optical intensity and phase modulation using fiber-integrated metasurfaces based on nanostructured subwavelength thickness phase change GST films deposited on fiber tips. The use of metasurfaces enables the tuning of the spectral position of the metasurface transmission resonances, by adjusting metamolecule geometry, enabling structurally engineered resonant operation anywhere within the transparency range of the GST alloy. This device concept is, furthermore, transferrable to other spectral bands and through using different metamolecules and/or other chalcogenide alloys can be used for non-volatile

control of a variety of different optical properties in all-fiber devices, including group velocity and polarization mode dispersion, for low power, all-optical long-range data transmission as well as reconfigurable channel multiplexing in emerging photonic lantern technologies. Moreover, such devices enable control over signal intensity and phase with built-in memory functionality, thus provide solutions well beyond purely telecommunication network applications. These devices unlock a range of exciting application in endoscopic imaging and smart textiles for wearable technologies to Lidar for autonomous vehicles and adaptive industrial process monitoring.

ACKNOWLEDGEMENTS

The authors would like to thank Prof Nikolay Zheludev for valuable discussions and input. This work was supported by the Canadian Natural Science and Engineering Research Council (NSERC), Engineering and Physical Sciences Research Council, UK [grant number EP/N00762X/1], and the Singapore Ministry of Education [MOE2016-T3-1-006]. Tiago Martins was partially supported by Fundação para a Ciência e Tecnologia under the grant PD/BD/135008/2017. Yihao Cui was supported by the Canadian Natural Sciences and Engineering Research Council and Alberta Innovates [NSERC RGPIN-2019-03952]. Tiago Martins and Yihao Cui contributed equally to this work.

The data from this paper can be obtained from the University of Alberta research repository: <https://doi.org/10.7939/r3-tdan-8m16>

References

[1] D. J. Richardson, J. M. Fini, L. E. Nelson, *Nature Photonics* 2013, 7, 354; G. Li, N. Bai, N. Zhao, C. Xia, *Advances in Optics and Photonics* 2014, 6, 4, 413.

[2] D. Piccinotti, K. F. MacDonald, S. A Gregory, I. Youngs, N. I. Zheludev, *Reports on Progress in Physics* 2020, 84, 1, 012401; J. Feldmann, N. Youngblood, C. D. Wright, H.

Bhaskaran, W. H. P. Pernice, *Nature* 2019, 569, 7755, 208-214.

[3] H. Zhang, S. B. Lu, J. Zheng, J. Du, S. C. Wen, D. Y. Tang, K. P. Loh, *Optics Express* 2014, 22, 6, 7249; J. M. Dudley, J. R. Taylor, *Nature Photonics* 2009, 3, 2, 85-90; S. Danto, Z. Ruff, Z. Wang, J. D. Joannopoulos, Y. Fink, *Advanced Functional Materials* 2011, 21, 6, 1095-1101.

[4] B. Gholipour, P. Bastock, L. Cui, C. Craig, K. Khan, D. W. Hewak, C. Soci, *Scientific Reports* 2016, 6, 35409; A. F. Abouraddy, M. Bayindir, G. Benoit, S. D. Hart, K. Kuriki, N. Orf, O. Shapira, F. Sorin, B. Temelkuran, Y. Fink, *Nat. Mater* 2007, 6, 5, 336-347; V. Savinov, N. I. Zheludev, *Applied Physics Letters* 2017, 111, 9, 091106.

[5] T. G. Martins, B. Gholipour, D. Piccinotti, K. F. MacDonald, A. C. Peacock, O. Frazão, N. I. Zheludev, *APL Photonics* 2019, 4, 111301.

[6] H. Zhang, N. Healy, A. F. J. Runge, C. C. Huang, D. W. Hewak, A. C. Peacock, *Optics Letters* 2018, 43, 13, 3100; Q. Bao, H. Zhang, B. Wang, Z. Ni, C. H. Y. X. Lim, Y. Wang, D. Y. Tang, K. P. Loh, *Nature Photonics* 2011, 5, 7, 411-415; A. Xomalis, I. Demirtzioglou, E. Plum, Y. Jung, V. Nalla, C. Lacava, K. F. MacDonald, P. Petropoulos, D. J. Richardson, N. I. Zheludev, *Nature Communications* 2018, 9, 182; Y. Zhao, J. Zhang, J. Du, J. Wang, *Applied Physics Letters* 2018, 113, 6, 061103.

[7] A. M. Urbas, Z. Jacob, L. Del Negro, N. Engheta, A. D. Boardman, P. Egan, A. B. Khanikaev, V. Menon, M. Ferrera, N. Kinsey, C. DeVault, J. Kim, V. Shalaev, A. Boltasseva, J. Valentine, C. Pfeiffer, A. Grbic, E. Narimanov, L. Zhu, S. Fan, A. Alù, E. Poutrina, N. M. Litchinitser, M. Naginov, K. F. MacDonald, E. Plum, X. Liu, P. Nealey, C. R. Kagan, C. B. Murray, D. A Pawlak, I. Smolyaninov, V. N. Smolyaninova and D. Chanda, *Journal of Optics* 2016, 18, 9, 093005.

[8] N. I. Zheludev, Y. S. Kivshar, *Nat Mater* 2012, 11, 11, 917-924.

[9] M. I. Stockman, K. Kneipp, S. I. Bozhevolnyi, S. Saha, A. Dutta, J. Ndukaife, N. Kinsey, H. Reddy, U. Guler, V. M. Shalae, A. Boltasseva, B. Gholipour, H. N. S. Krishnamoorthy, K. F. MacDonald, C. Soci, N. I. Zheludev, V. Savinov, R. Singh, P. Groß, C. Lienau, M. Vadai, M. L. Solomon, D. R. Barton, M. Lawrence, J. A. Dionne, S. V. Boriskina, R. Esteban, J. Aizpurua, X. Zhang, S. Yang, D. Wang, W. Wang, T. W. Odom, N. Accanto, P. M. de Roque, I. M. Hancu, L. Piatkowski, N. F. van Hulst, M. F. Kling, *Journal of Optics* 2018, 20, 4, 043001; J. Perkins, B. Gholipour, *Advanced Photonics Research* 2021, 2000141.

[10] B. J. Eggleton, B. Luther-Davies, K. Richardson, *Nat. Photon* 2011, 5, 3, 141-148; C.-C. Huang, F. Al-Saab, Y. Wang, J.-Y. Ou, J. C. Walker, S. Wang, B. Gholipour, R. E. Simpson, D. W. Hewak, *Nanoscale* 2014, 6, 21, 12792-12797.

[11] C. C. Huang, B. Gholipour, J. Y. Ou, K. Knight, D. W. Hewak, *Electron. Lett.* 2011, 47, 4, 288; M. A. Hughes, Y. Fedorenko, R. M. Gwilliam, K. P. Homewood, S. Hinder, B. Gholipour, D. W. Hewak, T.-H. Lee, S. R. Elliott, R. J. Curry, *Appl. Phys. Lett.* 2014, 105, 8, 083506; D. Loke, T. H. Lee, W. J. Wang, L. P. Shi, R. Zhao, Y. C. Yeo, T. C. Chong, S. R. Elliott, *Science* 2012, 336, 6088, 1566-1569; M. Wuttig, N. Yamada, *Nat Mater* 2007, 6, 12, 1004-1004.

[12] M. A. Hughes, Y. Fedorenko, B. Gholipour, J. Yao, T.-H. Lee, R. M. Gwilliam, K. P. Homewood, S. Hinder, D. W. Hewak, S. R. Elliott, R. J. Curry, *Nature Communications* 2014, 5, 5346.

[13] S. Kasap, *Springer handbook of electronic and photonic Materials*, Springer International Publishing, 2017.

[14] D. Piccinotti, B. Gholipour, J. Yao, K. F. MacDonald, B. E. Hayden, N. I. Zheludev, *Advanced Materials* 2019, 1807083; D. Piccinotti, B. Gholipour, J. Yao, K. F. Macdonald, B. E. Hayden, N. I. Zheludev, *Optics Express* 2018, 26, 16, 20861.

[15] F. F. Schlich, P. Zalden, A. M. Lindenberg, R. Spolenak, ACS Photonics 2015, 2, 2, 178-182; K. B. Borisenko, J. Shanmugam, B. A. O. Williams, P. Ewart, B. Gholipour, D. W. Hewak, R. Hussain, T. Javorfi, G. Siligardi, A. I. Kirkland, Scientific Reports 2015, 5, 1; B. Gholipour, Science 2019, 366, 6462, 186.

[16] Y. Zhang, C. Fowler, J. Liang, B. Azhar, M. Y. Shalaginov, S. Deckoff-Jones, S. An, J. B. Chou, C. M. Roberts, V. Liberman, M. Kang, C. Ríos, K. A. Richardson, C. Rivero-Baleine, T. Gu, H. Zhang, J. Hu, Nature Nanotechnology 2021, 16, 6, 661-666; F. Zhang, X. Xie, M. Pu, Y. Guo, X. Ma, X. Li, J. Luo, Q. He, H. Yu, X. Luo, Advanced Materials 2020, 32, 39, 1908194; Y. Wang, P. Landreman, D. Schoen, K. Okabe, A. Marshall, U. Celano, H. S. P. Wong, J. Park, M. L. Brongersma, Nature Nanotechnology 2021, 16, 6, 667-672; A. Karvounis, B. Gholipour, K. F. MacDonald, N. I. Zheludev, Appl. Phys. Lett. 2016, 109, 5, 051103; H. N. S. Krishnamoorthy, B. Gholipour, N. I. Zheludev, C. Soci, Adv. Opt. Mater 2018, 1800332; A.-K. U. Michel, A. Heßler, S. Meyer, J. Pries, Y. Yu, T. Kalix, M. Lewin, J. Hanss, A. De Rose, T. W. W. Maß, M. Wuttig, D. N. Chigrin, T. Taubner, Advanced Materials 2019, 31, 29, 1901033; B. Gholipour, D. Piccinotti, A. Karvounis, K. F. MacDonald, N. I. Zheludev, Nano Letters 2019, 19, 3, 1643-1648; A. C. Mandal, Yihao; McRae, Liam; Gholipour, Behrad, Journal of Physics: Photonics 2021, 3, 022005; B. Gholipour, J. Zhang, K. F. MacDonald, D. W. Hewak, N. I. Zheludev, Adv. Mater 2013, 25, 22, 3050-3054.

[17] B. Gholipour, A. Karvounis, J. Yin, C. Soci, K. F. Macdonald, N. I. Zheludev, NPG Asia Mater. 2018, 10, 533-539.

Supporting information

Fiber-integrated phase change metasurfaces with switchable group delay dispersion

Tiago Martins^{1, 2*}, Yihao Cui^{3*}, Behrad Gholipour^{2, 3, 4†}, Jun-Yu Ou², O. Frazão¹ and Kevin F. MacDonald²

¹ INESC TEC and Department of Physics and Astronomy, Faculty of Sciences, University of Porto, Rua do Campo Alegre, 687, 4150-179 Porto, Portugal

² Optoelectronics Research Centre and Centre for Photonic Metamaterials, University of Southampton, Southampton, SO17 1BJ, UK

³ Department of Electrical and Computer Engineering, University of Alberta, Canada, T6G 1H9

⁴ Department of Chemistry, University of Southampton, Southampton, SO17 1BJ, UK

* Contributed equally to this work

† Corresponding author: bgholipo@ualberta.ca

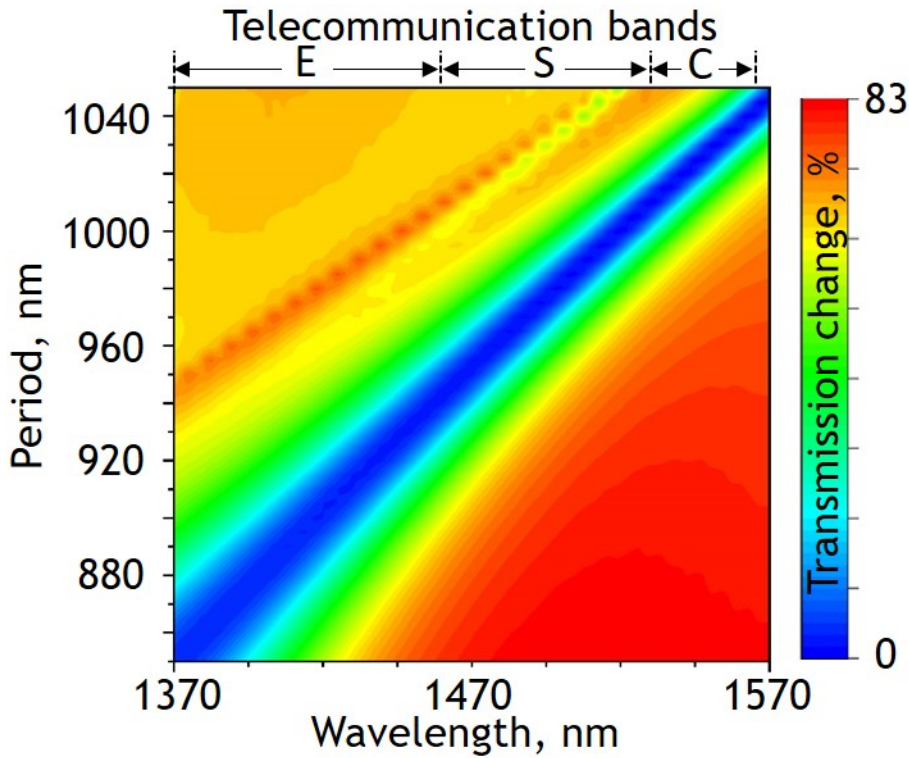


Figure S1: Numerically simulated change in transmission between amorphous and crystalline phases for metasurfaces ranging from 850nm to 1050nm periods.

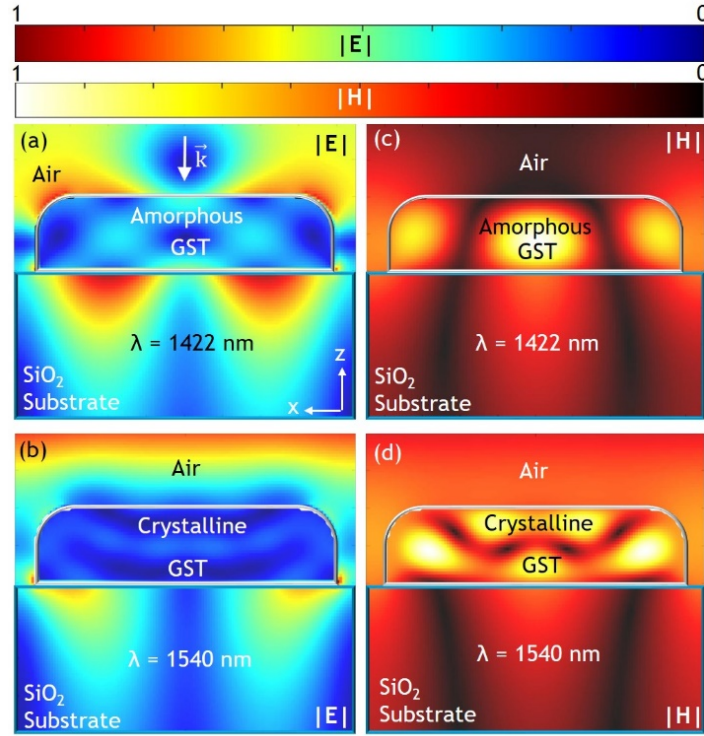
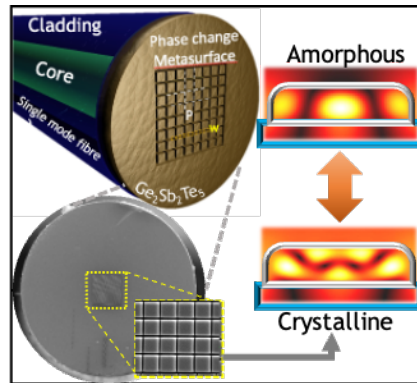


Figure S2. (a, b) Electric and (c, d) magnetic field distribution of a metasurface with $w = 80$ nm, $t = 200$ nm and $P = 900$ nm, in the amorphous (a, c) and (b, d) crystalline phases; plotted at their respective resonance wavelength.

Table of Content (TOC) image:



TOC text: Light-induced amorphous-crystalline phase switching in a chalcogenide metasurface, fabricated on the end-facet of a single mode optical fiber, enables intensity and phase modulation of the guided wave at metasurface designated bands. Such devices present a range of opportunities in fiberized remotely programmable phase/intensity multiplexing and dynamic dispersion compensation for emerging telecommunications and data storage/processing applications.